Title Page

Physiologically Based Pharmacokinetic Modeling of Bosentan Identifies the Saturable

Hepatic Uptake as A Major Contributor to Its Nonlinear Pharmacokinetics

Masanobu Sato, Kota Toshimoto, Atsuko Tomaru, Takashi Yoshikado, Yuta Tanaka,

Akihiro Hisaka, Wooin Lee and Yuichi Sugiyama

Advanced Review with Electronic Data Promotion Group, Pharmaceuticals & Medical

Devices Agency, Tokyo, Japan (M.S.); Sugiyama Laboratory, RIKEN Innovation

Center, Research Cluster for Innovation, RIKEN, Kanagawa, Japan (K.T., A.T., T.Y.,

Y.S.); DMPK Research Laboratory, Watarase Research Center, Kyorin Pharmaceutical

Co., Ltd., Tochigi, Japan (Y.T); Graduate School and Faculty of Pharmaceutical

Sciences, Chiba University, Chiba, Japan (A.H.); and College of Pharmacy, Research

Institute of Pharmaceutical Sciences, Seoul National University, Seoul, Korea (W.L.)

Running Title Page

Running title:

PBPK modeling of nonlinear PK of bosentan after IV dosing

Corresponding author:

Dr. Yuichi Sugiyama

1-7-22 Suehiro-cho, Tsurumi-ku, Yokohama, Kanagawa, 230-0045, Japan

Tel: +81-(0)45-503-9210

Fax: +81-(0)45-506-9190

ychi.sugiyama@riken.jp

The number of text page: 21

The number of tables: 3

The number of figures: 5

The number of references: 42

The number of words in Abstract: 222

The number of words in Introduction: 584

The number of words in Discussion: 1454

List of nonstandard abbreviations:

AUC, area under the curve; $CL_{int,met}$, hepatic intrinsic metabolic clearance; C_{max}, maximum concentration; CYPs, cytochrome P450; f_B, unbound fraction in blood; f_H, hepatic intracellular unbound fraction; K_P, partition coefficient; OATPs, organic anion transporting polypeptides; PBPK, physiologically based pharmacokinetic; PS_{act}, transporter-mediated active uptake clearance; PS_{dif}, passive diffusion clearance; Q_t, blood flow rate to tissue

Abstract

Bosentan is a substrate of hepatic uptake transporter organic anion transporting polypeptides (OATPs), and undergoes extensive hepatic metabolism by cytochrome P450 (CYPs), namely, CYP3A4 and CYP2C9. Several clinical investigations have reported a nonlinear relationship between bosentan doses and its systemic exposure, which likely involves the saturation of OATP-mediated uptake, CYP-mediated metabolism, or both in the liver. Yet, the underlying causes for the nonlinear bosentan pharmacokinetics are not fully delineated. To address this, we performed physiologically based pharmacokinetic (PBPK) modeling analyses for bosentan after its iv administration at different doses. As a bottom-up approach, PBPK modeling analyses were performed using *in vitro* kinetic parameters, other relevant parameters and scaling factors. As top-down approaches, three different types of PBPK models that incorporate the saturation of hepatic uptake, metabolism or both were compared. The prediction from the bottom-up approach (Models 1 and 2) yielded the blood bosentan concentration-time profiles and its systemic clearance values that are not in good agreement with the clinically observed data. From top-down approaches (Models 3, 4, 5-1 and 5-2), the prediction accuracy was best only with the incorporation of the saturable hepatic uptake for bosentan. Taken together, the PBPK models for bosentan were successfully established and comparison of different PBPK models identified the saturation of the hepatic uptake process as a major contributing factor for the nonlinear pharmacokinetics of bosentan.

4

Introduction

Bosentan is a dual endothelin-receptor antagonist and indicated for the treatment of patients with pulmonary arterial hypertension (Rubin et al., 2002; Dingemanse and van Giersbergen, 2004; Galiè et al., 2008). Several clinical investigations have so far reported apparently opposing results in regard to a nonlinear relationship between IV and oral administration of bosentan and its systemic exposure in humans. When single IV bosentan doses ranging from 10 to 750 mg were administered to healthy volunteers, the systemic plasma clearance of bosentan decreased with increasing doses (10.8 and 5.7 L/hr for the bosentan doses of 10 and 750 mg, respectively) (Weber et al., 1996). In the case of oral dosing, the systemic exposure of bosentan increased in a dose-proportional manner up to 600 mg bosentan doses in healthy volunteers. However, with bosentan oral doses greater than 600 mg, the fold increases in the systemic exposure (i.e. maximum concentrations (C_{max}), areas under the plasma concentration-time curve (AUCs)) were less than dose-proportional (Weber et al., 1996). Following repeated oral dosing of 500 mg bosentan, the plasma clearance of bosentan was increased by approximately 2-fold, accompanied by approximately 1.7-fold increase in 24-hour urinary excretion of 6β-hydrocycortisol, indicating auto-induction of bosentan metabolism mediated by cytochrome P450 (CYP) 3A4 (Weber et al., 1999a).

Bosentan has also been associated with various cases of drug interactions when coadministered with drugs that inhibit/induce some CYP enzymes and/or hepatic uptake transporter organic anion-transporting polypeptides (OATPs). For example, the systemic exposure of bosentan at the steady state was increased approximately 4- and 2-fold by co-

administration of clarithromycin and ketoconazole, respectively (Markert et al., 2014; van Giersbergen et al., 2002). Following the second concomitant dosing of bosentan with cyclosporine, average trough concentrations of bosentan were 31-fold higher than those after the first dosing of bosentan (Binet et al., 2000). In the case of rifampin coadministration, the changes in the bosentan pharmacokinetics depended on the number of rifampin dosing (van Giersbergen et al., 2007). The systemic exposure of bosentan markedly increased after the single rifampin dose coadministered, but significantly decreased after multiple rifampin doses. The cases of drug interactions are also reported for bosentan when coadministered with simvastatin (Dingemanse et al., 2003) and warfarin (Weber et al., 1999b). These complex drug interactions with bosentan likely involve the saturation of OATP-mediated uptake, CYP-mediated metabolism, or both in the liver, yet a detailed mechanistic understanding has been lacking.

Several clinical and non-clinical studies provided the evidence supporting the involvement of CYP enzymes and OATPs in the disposition of bosentan. A clinical study with ^{14}C-labeled bosentan indicated extensive hepatic elimination of bosentan with minor renal and fecal excretion (Weber et al., 1999c). The two major metabolites hydroxyl bosentan and desmethyl bosentan are reported to be produced mainly by CYP3A4/CYP2C9 and by CYP3A4, respectively (Dingemanse and van Giersbergen, 2004). Bosentan is also a substrate of OATP1B1, OATP1B3, and OATP2B1 (Treiber et al., 2007; Jones et al., 2012). In rats, pharmacokinetic interactions between bosentan and cyclosporine A were reported with the proposed mechanism involving the inhibition of hepatic uptake of bosentan by cyclosporine A (Treiber et al., 2004).

6

Physiologically based pharmacokinetic (PBPK) modeling has increasingly shown its utility in providing the kinetic and mechanistic insights into nonlinear pharmacokinetics and complex drug interactions (Fan et al., 2010; Watanabe et al., 2010; Rowland et al., 2011). In the current study, we developed PBPK models for analyzing the systemic nonlinear pharmacokinetics of bosentan after its iv administration at different doses by incorporating saturable processes of hepatic uptake, metabolism, or both via bottom-up and top-down approaches.

7

Materials and Methods

Materials

Bosentan was purchased from the Cayman Chemical Company (Ann Arbor, MI). Bosentan-d4, hydroxyl bosentan, and desmethyl bosentan were purchased from Toronto Research Chemicals Inc. (Ontario, Canada). Pooled cryopreserved human hepatocytes from 20 mixed-gender donors (Caucasian: 14, Hispanic: 4 and Black: 2) were purchased from Veritas (Tokyo, Japan). Pooled human liver microsomes from mixed-gender donors were purchased from Corning Japan (Tokyo, Japan). All other chemicals and reagents were readily available from commercial sources.

Kinetic parameters for bosentan uptake (human cryopreserved hepatocytes)

Uptake studies using human cryopreserved hepatocytes were performed using a rapid separation method as described previously (Shitara et al., 2003). Briefly, cryopreserved hepatocytes were thawed out, washed and resuspended in Krebs–Henseleit buffer (at the density of 2×10^6 cells/mL). After preincubation at 37°C for 5 min, bosentan uptake was initiated by adding an equal volume of bosentan-containing buffer (the final concentrations of 0.6, 3, 6, 10, 30, or 100 μM) to the hepatocyte suspensions. After incubation at 37°C for 0.5, 1.5, or 3 min, the reaction was terminated by separating the cells from the bosentan solution. The separation was performed using tubes containing 50 μL of 2.5 M ammonium acetate under a layer of 100 μL of oil mixture (density = 1.015, a mixture of silicone oil and mineral oil). Following centrifugation at $2,000 \times g$ for 30 sec, tubes were snap-frozen immediately and kept at -80°C until analysis. After thawing on

8

ice, the centrifuge tube was cut below the oil layer and cells were resuspended in 40 μL of water. This suspension was transferred to another tube containing an internal standard and acetonitrile, sonicated for 4.5 min using a Bioruptor device (Cosmo Bio Co., Ltd., Tokyo, Japan). After centrifugation at 15,000×g for 5 min, the resulting supernatant was diluted 2-fold with 0.1% formic and subjected to liquid chromatography/tandem mass spectrometry (LC-MS/MS) analysis. Bosentan uptake into the hepatocytes was expressed as the uptake volume of bosentan (μL/10^6 cells, the bosentan amount detected divided by the bosentan concentration in the assay buffer). The initial uptake velocity of bosentan was calculated from the slope of the uptake volume obtained from 0.5 to 3 min and was expressed as the uptake clearance (μL/min/10^6 cells). The kinetic parameters for the bosentan uptake of bosentan were calculated using the following equation:

$$v = \frac{V_{max,uptake} \times S}{K_{m.uptake} + S} + PS_{dif} \times S$$

(v, the initial uptake rate (pmol/min/10^6 cells); S, the substrate concentration (μM); $V_{max,uptake}$, the maximum uptake rate (pmol/min/10^6 cells); $K_{m,uptake}$, the Michaelis constant of uptake (μM); PS_{dif}, the passive diffusion clearance)

The hepatic intracellular unbound fraction (f_H) was calculated as described previously (Yoshikado et al., 2016). Briefly, the hepatocyte suspensions (2.0×10^6 cells/mL) were incubated with an equal volume of buffer containing bosentan (the final concentration, 1 μM) on ice for 0.5, 15, 30, or 60 min and cells were separated and processed using the same method described above. Bosentan levels in cell lysates and medium were quantified by LC-MS/MS. It was assumed that the active transport and membrane

9

potential were abolished on ice and that the protein unbound fraction in the medium was 1. Using the values at 60 min (when the uptake was presumed be at the steady state), f_H was calculated using the following equation.

$$\frac{C_{cell(-)}}{C_{medium(-)}} = \frac{C_{u,cell(-)}}{C_{u,medium(-)}} \times \frac{1}{f_H}$$

($C_{cell(-)}$ and $C_{medium(-)}$, total bosentan concentrations in the cell and medium measured on ice at 60 min, respectively; $C_{u,cell(-)}$ and $C_{u,medium(-)}$, unbound bosentan concentrations in the cell and medium, respectively).

Kinetic parameters for bosentan metabolism (human liver microsomes)

The kinetic parameters for bosentan metabolism were assessed by monitoring the generation of both hydroxyl bosentan and desmethyl bosentan. The reaction mixture was prepared with pooled human liver microsomes (the final concentration, 2 mg/mL) and 100 mM phosphate buffer containing bosentan (the final concentrations: 2, 4, 10, 25, 60, or 150 μM). After preincubation at 37°C for 5 min, the reaction was initiated by the addition of a NADPH-generating system (the final concentrations of 0.5 mM β-NADPH, 5 mM glucose 6-phosphate, 1 U/mL glucose-6-phosphate dehydrogenase, 3 mM $MgCl_2$). The reaction was terminated by the addition of two equivalent volumes of ice-cold, acetonitrile containing an internal standard, followed by brief vortexing. After centrifugation at 13,000×g for 10 min, the resulting supernatant was diluted with 0.1% formic acid and subjected to LC-MS/MS analysis.

$K_{m,met}$, $V_{max,met}$, and $CL_{met,nonsaturation}$ were calculated using the following equation (fitting was performed using the nonlinear least-squares method).

$$v = V_{max,met} \times \frac{S}{K_{m,met} + S} + CL_{met,nonsaturation} \times S$$

(v, the initial velocity (pmol/min/mg protein); S, the substrate concentration (μM); $V_{max,met}$, the maximum velocity of metabolism (pmol/min/mg protein); $K_{m,met}$, the Michaelis constant of metabolism (μM); $CL_{met,nonsaturation}$, nonsaturable metabolic clearance)

LC-MS/MS Analysis

To quantify bosentan, hydroxyl bosentan, and desmethyl bosentan, the LC-MS/MS analyses were performed using a Nexera X2 separating module (Shimadzu Co., Kyoto, Japan) equipped with an LCMS8040 mass spectrometer (Shimadzu Co.) with an electron ion spray interface. The mass spectrometer was operated in the multiple reaction monitoring mode using the respective MH^+ ions; m/z 552→m/z 202 for bosentan, m/z 568→m/z 202 for hydroxyl bosentan, m/z 538→m/z 494 for desmethyl bosentan, and m/z 556→m/z 202 for bosentan-d4. The mobile phase was 55% acetonitrile containing 0.1% formic acid, and the flow rate was 0.2 mL/min with the stationary phase, a C18 column (Kintex C18, 2.1 × 100 mm, 2.6 μm; Phenomenex Inc., Torrance, CA) at 40°C.

Parameter optimization by nonlinear least squares fitting

All fitting and simulation analyses were performed using a multiple-purpose nonlinear least squares fitting computer program Napp (version 2.31) (Hisaka and Sugiyama, 1998). Differential equations were numerically solved using the Runge–Kutta–Fehlberg method. To evaluate goodness of the fit, the sum of the weighted, squared residuals (WSS) and Akaike Information Criterion (AIC) were calculated using the following equations;

$$\text{WSS} = \sum_{i=1}^{n} \left(\frac{y_i - y'_i}{y_i} \right)^2$$

(y_i, the ith observed value; y'_i, the ith predicted value)

$$\text{AIC} = \text{nlnWSS} + 2\text{m}$$

(n, the number of observations; m, the number of estimated parameters in the model)

Structure of the PBPK models for bosentan

Figure 1 shows the structure of PBPK model for bosentan administered as an IV bolus. Similar to the basic model reported previously (Yoshikado et al., 2016), the current model consists of the central compartment connected with the liver. Given that bosentan is a lipophilic drug (LogPo:w is 3.4), our PBPK model included three large-volume tissues (i.e. adipose, muscle, skin) where lipophilic drugs tend to have considerable distribution. Rapid equilibrium distribution in these tissues was also assumed given that bosentan was reported neither for particularly slow tissue distribution nor for its interactions with transporters in non-hepatic organs. The partition coefficient between these tissues and blood (K_P) was calculated using the method reported by Rodgers and Rowland (Rodgers and Rowland, 2006). The liver compartment was divided into five units of extrahepatic

12

and hepatocellular compartments. Previously, this 5-compartment liver model was shown to mimic the realistic hepatic disposition based on the dispersion model while it is mathematically simpler than the dispersion model (Watanabe et al., 2007). Extrahepatic compartments were linked tandemly by blood flow, and transporter-mediated active uptake clearance (PS_{act}) and passive diffusion influx clearance ($PS_{dif,inf}$) as well as passive diffusion efflux clearance ($PS_{dif,eff}$) were incorporated. It was assumed that hepatic uptake intrinsic clearance is determined by the sum of PS_{act} and $PS_{dif,inf}$, and that hepatic intrinsic efflux clearance from hepatocytes to blood is determined by $PS_{dif,eff}$. Hepatic intrinsic metabolic clearance ($CL_{int,met}$) was incorporated in each hepatocellular compartment. Renal clearance (CL_r) from the central compartment was also incorporated, although CL_r is much lower than nonrenal clearance (f_e is about 0.008 in human) (Weber et al., 1996). Although bosentan was reported to be a substrate of MRP2 (Fahrmayr et al., 2013), active efflux from hepatocytes into bile was not included in the PBPK model. This was based on the reports suggesting that MRP2-mediated efflux may play a minimal role on bosentan PK in humans: 4% of bosentan dose was found in feces as an unchanged form after IV dosing in healthy volunteers (Weber et al., 1999b) and the absolute bioavailability of bosentan is ~0.5 (Weber et al., 1996a). Differential equations for the constructed PBPK model are provided in the **Supplementary text 1**.

All physiological and kinetic parameters used are listed in Table 1. Tissue volume was converted to tissue weight with the assumption that the tissue density is 1 g/mL. Unbound fraction in liver (f_H) is fixed at the value determined by *in vitro* study on ice, which is shown to be consistent with that estimated at 37°C using human liver homogenates

13

(Yoshikado et al., 2017). In all analyses conducted in this study, $PS_{dif,eff}$ was calculated by the following equation described previously (Yoshikado et al., 2016);

$$PS_{dif,eff} = \frac{PS_{dif,inf}}{\gamma}$$

The γ value was calculated to be 0.243 at 37°C with consideration of the followings: i) the ratio of the membrane permeability by passive diffusion of an ionized form of the drug to that of its unionized form (obtained from *in vitro* experiments that examine pH-dependent membrane permeability); ii) the concentration ratio of an ionized form of the drug to its unionized form, derived from the Henderson-Hasselbalch equation (intracellular pH=7.2, extracellular pH=7.4); and iii) the membrane potential estimated from the Nernst equation (Yoshikado et al., 2016).

Both bottom-up and top-down approaches were used for the current PBPK modeling analyses (summarized in Table 2). As bottom-up approaches, simulation analyses were performed using the kinetic parameters extrapolated from *in vitro* to *in vivo* using biological scaling factors (Model 1) or those obtained by fitting (Model 2). Detailed description on the handling of various parameters is included in the **Supplementary text 1**. As top-down approaches (Models 3, 4 and 5), we performed simultaneous fitting analyses of the PBPK models that incorporate saturation processes for PS_{act}, $CL_{int,met}$ or both to blood bosentan concentration-time profiles using the following equations.

PS_{act} saturation model (Models 3 and 5):

$$PS_{act} = \frac{In\ vivo\ V_{max,uptake}}{In\ vivo\ K_{m,uptake} + f_B C_{HEi}}$$

$CL_{int,met}$ saturation model (Models 4 and 5):

$$CL_{int,met} = \frac{In\ vivo\ V_{max,met}}{In\ vivo\ K_{m,met} + f_H C_{HCi}}$$

Tables 2 and 3 summarize the characteristics of the PBPK models used and the initial value as well as lower and upper limits (range) of each parameter for optimizing kinetic parameters, respectively.

Monte Carlo simulation of bosentan blood concentration profiles

One set of blood bosentan concentration-time profiles for 6 virtual subjects (same as the previous report (Weber et al., 1996)) were generated from Monte Carlo simulation based on the constructed PBPK model (Model 3), and the same process was repeated for 40 times to generate additional sets. The coefficient of variation (CV) values for *in vivo V*$_{\text{max,uptake}}$, *in vivo K*$_{\text{m,uptake}}$, and *in vivo PS*$_{\text{dif}}$ (those displaying inter-individual variability) were set as 25.8%, 25.8%, and 10% as per the previously reported modeling methodologies (Kato et al., 2003, Ito et al., 2017 and Toshimoto et al., 2017), and that for *in vivo CL*$_{\text{met}}$ was set as 33%, as reported previously (Kato et al., 2010). For parameters displaying intra-individual variability, propotional CV values were set as 24.8% (Volz et al., 2017). The *in vivo V*$_{\text{max,uptake}}$, *in vivo K*$_{\text{m,uptake}}$, *in vivo PS*$_{\text{dif}}$, and *in vivo CL*$_{\text{met}}$ parameters were assumed to follow a log-normal distribution.

15

Results

Kinetic parameters of bosentan uptake and metabolism from *in vitro* studies

The uptake of bosentan by human hepatocytes was proportional to time at least up to

for 3 min after the onset of incubation in all bosentan concentrations (data not shown).

Thus, the uptake rates were calculated from this linear part of the time-uptake curves

using differing bosentan concentrations and used to prepare the Eadie–Hofstee plot (Fig.

2) and to obtain the kinetic parameters (Table 1). PS_{act} (calculated from V_{max}/K_m under the

unsaturated conditions) was 35.6 μL/min/10^6 cells, approximately 12 times higher than

$PS_{dif,inf}$. The hepatic intracellular unbound fraction (f_H), was obtained from the steady-

state uptake study under ice-cold conditions and determined to be 0.0696 ± 0.0068 (Table

1). Similarly, the Eadie-Hofstee plots and the kinetic parameters for the production of

hydroxyl bosentan and desmethyl bosentan by human liver microsomes were obtained

(Fig. 3 and Table 1). Under the unsaturated condition, the *in vitro* intrinsic metabolic

clearance for the production of hydroxyl bosentan and desmethyl bosentan (calculated

from V_{max}/K_m) were 2.56 and 1.57 μL/min/mg of microsomal protein, respectively.

PBPK modeling via bottom-up approaches (Models 1 and 2)

For Model 1, the blood concentration-time profiles of bosentan were simulated using

the kinetic parameters of hepatic uptake and metabolism obtained from *in vitro* studies

and extrapolated using biological scaling factors. The predicted blood concentrations of

bosentan were consistently higher than the reported values at nearly all time points for

16

every dose level (Fig. 4a), resulting in the under-prediction of the total body clearances compared to the observed *in vivo* values.

Instead of biological scaling factors, Model 2 utilized scaling factors that were optimized by fitting. With this modification, the predicted values of dose-normalized AUCs became closer to the reported values. However, the blood bosentan concentration-time profiles simulated by Model 2 were not in good agreement with the clinically observed data (Fig. 4b).

PBPK modeling via top-down approaches (Models 3, 4 and 5)

The next three PBPK models incorporated the saturable processes for hepatic uptake only (Model 3), metabolism only (Model 4), or both (Models 5). Model 3 yielded the predicted profiles that were in good agreement with the observed values as well as the smallest AIC values among the tested models (Fig. 4c and Table 3). Models 4, which incorporated the saturable process for hepatic metabolism only, yielded the profiles that substantially deviated from the clinically observed data, especially at early times at high doses of bosentan (Fig. 4d). Model 5, which incorporated the saturable process for both hepatic uptake and metabolism, the simulated blood concentration-time profiles of bosentan were in much better agreement with the observed data than those predicted from Model 4 (Fig. 4e). The AIC value also substantially improved from 125 (Model 4) to 86.8 (Model 5).

Monte Carlo simulation of PBPK modeling

17

Taking inter-individual and intra-individual variability of the parameters of Model 3 into consideration, Monte Carlo simulations were carried out. The simulated dose-normalized AUCs of every dose level were similar to the reported values, in terms of the average and standard error (Fig. 5). These results suggest that the variation in AUCs after IV bosentan dosing may be explained mostly by the variation in the kinetic processes of hepatic uptake and metabolism.

Discussion

In our current study, the PBPK models for bosentan were developed to enhance our kinetic and mechanistic understanding of nonlinear pharmacokinetics associated with bosentan therapy. Based on the results comparing different PBPK models (Models 1-5), the saturable hepatic uptake of bosentan is a most likely contributor to nonlinear pharmacokinetics of intravenously administered bosentan.

In order to obtain kinetic parameters necessary for our PBPK modeling analyses, we assessed the processes of both hepatic uptake and metabolism of bosentan in the current study. The *in vitro* $K_{m,uptake}$ value for bosentan was determined to be 1.33 μM using suspended human cryopreserved hepatocytes and was considered to be in the comparable range with the previously reported values using OATP1B1-expressing cells or sandwich-cultured hepatocytes (4.27-44 μM) (Jones et al., 2012, Ménochet et al., 2012, Izumi et al., 2015). And the *in vitro* $K_{m,met}$ values for the production of hydroxyl bosentan and desmethyl bosentan were determined to be 6.40 and 4.80 μM, respectively, using pooled human liver microsomes. The K_m values for bosentan metabolism was 12.3-232 μM using recombinant CYP2C9 microsomes (Chen et al., 2014) or 13 μM using human liver microsome (Ubeaud et al., 1995). The K_m values in our experiment appear comparable with the previous reports. By using the method reported previously (Hallifax and Houston, 2006), the lipophilicity of bosentan and the experimental conditions used in our *in vitro* study, the unbound fraction (fu_{inc}) of bosentan was predicted to be 0.867 for in the presence of microsomal protein 2 mg/ml. This prediction results suggested that the microsomal protein binding of bosentan may not be so extensive in our experimental

19

conditions.

These K_m values for bosentan metabolism and uptake were comparable with the estimated unbound maximum bosentan blood concentration (over 5 μM) in healthy volunteers after receiving the IV bosentan 750 mg dose. The *in vitro* V_{max}/K_m value for bosentan uptake (using pooled human cryopreserved hepatocytes) was 35.6 μL/min/10^6 cells, approximately 12 times higher than the *in vivo* PS_{dif} value (2.89 μL/min/10^6 cells) (Table 1). These results indicate that bosentan is actively taken up into the liver from the blood in humans and the unbound bosentan concentrations are likely to be higher in the hepatocytes than in human blood. These considerations provide justifications for further interrogating the saturation of hepatic uptake and/or metabolism of bosentan as possible underlying mechanisms for nonlinear bosentan pharmacokinetics.

For Model 1 (a bottom-up approach with the use of biological scaling factors), simulated bosentan blood concentration-time profiles and dose-normalized AUCs of bosentan substantially differed from the clinically observed data (Fig. 4a). When the kinetic parameters were scaled up to fit the clinically observed data (Model 2), the prediction accuracy improved for dose-normalized AUC values, yet substantial deviations in terms of bosentan blood concentration-time profiles (Fig. 4b). These findings may suggest that the scaling factors for *in vitro* $V_{max,uptake}/K_{m,uptake}$ and *in vitro* PS_{dif} need to be individually optimized instead of using a single scaling factor for both parameters. These findings are in line with the previous reports, which proposed that the scaling factor for OATP-mediated uptake clearance should be greater than 1 and be determined independently from *in vitro* PS_{dif} (Kusuhara and Sugiyama, 2009, Jones et al.,

20

2012 and Varma et al., 2014).

Among the PBPK models of top-down approaches, Model 3 was deemed to yield the best fit to the clinically observed data based on the AIC values. The scaling factors for bosentan uptake were calculated by calculating the ratio of the *in vivo* $V_{max,uptake}/K_{m,uptake}$ value to the biologically-scaled *in vitro* $V_{max,uptake}/K_{m,uptake}$ value (483 L/hr/78 kg), yielding 6.24, 4.89, and 5.43 for the models 3, 4, and 5, respectively. The reported scaling factors of OATP substrates, calculated using the same method, displayed considerable variability: 12 - 161 (Jones et al., 2012) or 1.0 - 101.8 (Varma et al., 2014). The scaling factors in our models appear to be less variable than those reported in the literature.

When the *in vivo* $K_{m,uptake}$ value of 0.534 or 0.667 μM was obtained by fitting in model 3 or 5, respectively, which were similar to the experimentally obtained *in vitro* $K_{m,uptake}$ value of 1.33 μM), simulated bosentan blood concentration-time profiles were in good agreement with the clinically observed data (Fig. 4). The similarity between *in vivo* and *in vitro* $K_{m,uptake}$ values may further support the saturation of hepatic uptake as a most likely contributor to the nonlinear pharmacokinetics of bosentan after IV dosing.

PBPK modeling analyses incorporating saturable hepatic metabolism yielded the $K_{m,met}$ values of 108 and 163 μM for Models 4 and 5, respectively. The maximum unbound concentrations of bosentan in the liver was predicted to be approximately 65 μM and 45 μM based on the simulation results using Models 4 and 5, respectively (Supplementary Figure 1) and the unbound fraction in hepatocytes (0.0696) obtained by our *in vitro* study. Therefore, we reasoned that saturation of bosentan metabolism in the liver is unlikely to occur at clinical relevant concentrations.

21

The $K_{m,met}$ values derived from models 4 (108 μM) and 5 (163 μM) differed from our

in vitro experiment results using HLM ($K_{m, met,OH}$ was 6.40 ± 1.20 μM and $K_{m, met,DES}$ was

4.80 ± 2.61 μM, respectively). These discrepancies may be related to the effects of

CYP2C9 polymorphism on bosentan metabolism. Chen *et al*. reported that the K_m values

for hydroxy bosentan production mediated by CYP2C9 vary widely from 12.3 to 232 μM

depending on CYP2C9 polymorphism (Chen *et al*., 2014). We were not able to further

investigate this possibility due to the limited information on CYP2C9 polymorphism of

the study participants.

The results of the Monte Carlo simulation also demonstrated that the variation in the

systemic exposure (AUCs) after bosentan IV dosing can be explained mostly by the

variations in $V_{max,uptake}$, $K_{m,uptake}$, PS_{dif} and $CL_{int,met}$ (Fig. 5).

We initially attempted the PBPK analyses of the nonlinear PK of bosentan after IV and

oral dosing at the same time. Different from the IV data, the dose-normalized AUC values

(AUC/dose) decreased with escalating oral doses of bosentan (Weber et al., 1996a). In

order to describe nonlinear PK after oral administration, PBPK models included the

components for solubility-limited absorption and saturable intestinal absorption mediated

by OATP2B1 (detailed information provided as Supplementary Files; Supplementary

Text 2, Supplementary Figures 2-7 and Supplementary Tables). Currently, we have

limited confidence in our PBPK models for oral bosentan data, mainly due to the lack of

information on excipients used for making bosentan suspensions. Further investigations

are warranted to establish reliable PBPK models for PO bosentan data. Very recently, the

PBPK models, which described IV and oral data of bosentan, has been reported (Li et al.,

22

2018). The results from our current study provide new information that saturation of hepatic uptake, but not of hepatic metabolism likely contributes to nonlinear PK after bosentan IV dosing.

Nonlinear bosentan PK was recently described by a two-compartment, target mediated drug disposition (TMDD) model (Volz et al., 2017). This model showed that bosentan binds to endothelin (ET) receptors with high affinity (K_d, ~1.9 nM), comparable to the measured binding constant (0.79–1.1 nM). In addition, the study reported that the receptor binding of bosentan is saturated with escalating doses (>50 mg IV). However, such findings differ from the reported clinical data where the systemic plasma clearance of bosentan decreased with escalating IV doses (11.5, 7.9, 6.4, and 4.8 L/h for IV bosentan doses of 50, 250, 500, and 750 mg, respectively) (Clin Pharmacol Ther. 1996; 60(2):124–137). Currently, the reasons for these apparent discrepancies are unknown. We are not aware of solid experimental evidence showing the internalization of the bosentan–ET receptor complex. For other ET receptor antagonists such as ambrisentan and macitentan, there is no report that they undergo TMDD. We thus believe that further efforts may be needed to determine the necessity of including TMDD in the bosentan PBPK model.

On the other hand, the K_m value (0.534 μM) for hepatic uptake derived from in our current PBPK model was comparable to that (1.33 μM) obtained from *in vitro* experiments. After 250 mg bosentan IV dosing, a maximum unbound bosentan concentration in blood was calculated as ~1.4 μM. Thus, it is reasonable to interpret that hepatic uptake of bosentan may be saturated with IV doses greater than 250 mg, affecting bosentan PK. Further investigation is warranted to examine the contribution of TMDD

23

on nonlinear PK of bosentan, but saturation of hepatic uptake appears to be a plausible mechanism for nonlinear PK of bosentan with high IV bosentan doses.

In conclusion, we established a PBPK model that can account for the nonlinear pharmacokinetics of intravenously administered bosentan by incorporating the saturable process of transporter-mediated hepatic uptake. The PBPK model established in this study may prove useful in explaining and predicting complex pharmacokinetic behaviors of bosentan and drug-drug interactions.

Acknowledgement

The authors acknowledge the following scientists for giving us useful advices in performing the analyses of oral administration data using Simcyp; Drs. Sibylle Neuhoff, Shriram Pathak, Matthew Harwood in Simcyp Certara and Dr.Amin Rostami in the University of Manchester.

Authorship Contributions

Participated in research design: Sato, Toshimoto, Tanaka, Hisaka, and Sugiyama

Conducted experiments: Tomaru

Performed data analysis: Sato, Tomaru, and Tanaka

Wrote or contributed to the writing of the manuscript: Sato, Lee, Toshimoto, Yoshikado,

Tomaru, and Sugiyama

References

Binet I, Wallnöfer A, Weber C, Jones R, Thiel G (2000) Renal hemodynamics and pharmacokinetics of bosentan with and without cyclosporine A. *Kidney Int* **57**: 224-31.

Chen M, Zhang Y, Pan P, Wang L, Zhan Y, Jin H, Xia M, Wang X, Dai D, Cai J, Hu G (2014) Effects of cytochrome P450 2C9 polymorphism on bosentan metabolism. *Drug Metab Dispos* **42**: 1820-5

Davies B and Morris T (1993) Physiological parameters in laboratory animals and humans. *Pharm Res* **10**: 1093-5.

Dingemanse J and van Giersbergen PL (2004) Clinical pharmacology of bosentan, a dual endothelin receptor antagonist. *Clin Pharmacokinet* **43**: 1089-115.

Dingemanse J, Schaarschmidt D, van Giersbergen PL (2003) Investigation of the mutual pharmacokinetic interactions between bosentan, a dual endothelin receptor antagonist, and simvastatin. *Clin Pharmacokinet* **42**: 293-301.

Fan J, Chen S, Chow EC, Pang KS (2010) PBPK modeling of intestinal and liver enzymes and transporters in drug absorption and sequential metabolism. *Curr Drug Metab* **11**: 743-61.

Fahrmayr C, König J, Auge D, Mieth M, Münch K, Segrestaa J, Pfeifer T, Treiber A, Fromm M (2013) Phase I and II metabolism and MRP2-mediated export of bosentan in a MDCKII-OATP1B1-CYP3A4-UGT1A1-MRP2 quadruple-transfected cell line. *Br J Pharmacol* **169**: 21-33.

27

Galiè N, Rubin Lj, Hoeper M, Jansa P, Al-Hiti H, Meyer G, Chiossi E, Kusic-Pajic A, and Simonneau G (2008) Treatment of patients with mildly symptomatic pulmonary arterial hypertension with bosentan (EARLY study): a double-blind, randomised controlled trial. *Lancet* **371**: 2093-100.

Hallifax D and Houston JB (2006) Binding of drugs to hepatic microsomes: comment and assessment of current prediction methodology with recommendation for improvement. *Drug Metab Dispos* **34**: 724-6

Hisaka A and Sugiyama Y (1998) Analysis of nonlinear and nonsteady state hepatic extraction with the dispersion model using the finite difference method. *J Pharmacokinet Biopharm* **26**: 495-519.

Ito M, Kusuhara H, Ose A, Kondo T, Tanabe K, Nakayama H, Horita S, Fujita T, Sugiyama Y (2017) Pharmacokinetic modeling and Monte Carlo simulation to predict interindividual variability in human exposure to oseltamivir and its active metabolite, Ro 64-0802. *AAPS J* **19**: 286-297.

Iwatsubo T, Hirota N, Ooie T, Suzuki H, Shimada N, Chiba K, Ishizaki T, Green CE, Tyson CA, Sugiyama Y (1997) Prediction of in vivo drug metabolism in the human liver from in vitro metabolism data. *Pharmacol Ther* **73**: 147-71.

Izumi S, Nozaki Y, Maeda K, Komori T, Takenaka O, Kusuhara H, Sugiyama Y (2015) Investigation of the impact of substrate selection on in vitro organic anion transporting polypeptide 1B1 inhibition profiles for the prediction of drug-drug interactions. *Drug Metab Dispos* **43**: 235-47.

Jamei M, Dickinson GL, Rostami-Hodjegan A (2009) A framework for assessing inter-individual variability in pharmacokinetics using virtual human populations and integrating general knowledge of physical chemistry, biology, anatomy, physiology and genetics: A tale of 'bottom-up' vs 'top-down' recognition of covariates. *Drug Metab Pharmacokinet* **24**: 53-75.

Jones HM, Barton HA, Lai Y, Bi YA, Kimoto E, Kempshall S, Tate SC, El-Kattan A, Houston JB, Galetin A, Fenner KS (2012) Mechanistic pharmacokinetic modeling for the prediction of transporter-mediated disposition in humans from sandwich culture human hepatocyte data. *Drug Metab Dispos* **40**: 1007-17.

Kato M, Tachibana T, Ito K, Sugiyama Y (2003) Evaluation of methods for predicting drug-drug interactions by Monte Carlo simulation. *Drug Metab Pharmacokinet* **18**: 121-7.

Kato M, Chiba K, Ito T, Koue T, Sugiyama Y (2010) Prediction of interindividual variability in pharmacokinetics for CYP3A4 substrates in humans. *Drug Metab Pharmacokinet* **25**: 367-78.

Kusuhara H and Sugiyama Y (2009) In vitro-in vivo extrapolation of transporter-mediated clearance in the liver and kidney. *Drug Metab Pharmacokinet* **24**:37-52.

Li R, Niosi M, Johnson N, Tess DA, Kimoto E, Lin J, Yang X, Riccardi KA, Ryu S, El-Kattan AF, Maurer TS, Tremaine LM, Di L (2018) A study on pharmacokinetics of bosentan with systems modeling, Part 1: translating systemic plasma concentration to liver exposure in healthy subjects. *Drug Metab Dispos* doi: 10.1124/dmd.117.078790

Markert C, Schweizer Y, Hellwig R, Wirsching T, Riedel KD, Burhenne J, Weiss J, Mikus G, Haefeli WE (2014) Clarithromycin substantially increases steady-state bosentan exposure in healthy volunteers. *Br J Clin Pharmacol* **77**: 141-8.

Ménochet K, Kenworthy KE, Houston JB, Galetin A (2012) Use of Mechanistic Modeling to Assess Interindividual Variability and Interspecies Differences in Active Uptake in Human and Rat Hepatocytes. *Drug Metab Dispos* **40**: 1744-56.

Rodgers T and Rowland M (2006) Physiologically based pharmacokinetic modelling 2: predicting the tissue distribution of acids, very weak bases, neutrals and zwitterions. *J Pharm Sci* **95**: 1238-57.

Rostami-Hodjegan A, Tucker GT (2007) Simulation and prediction of in vivo drug metabolism in human populations from in vitro data. *Nat Rev Drug Discov* **6**: 140-8.

Rowland M, Peck C, Tucker G (2011) Physiologically-based pharmacokinetics in drug development and regulatory science. *Annu Rev Pharmacol Toxicol* **51**: 45-73.

Rubin LJ, Badesch DB, Barst RJ, Galie N, Black CM, Keogh A, Pulido T, Frost A, Roux S, Leconte I, Landzberg M, and Simonneau G (2002) Bosentan therapy for pulmonary arterial hypertension. *N Engl J Med* **346**: 896-903

Shitara Y, Itoh T, Sato H, Li AP, Sugiyama Y (2003) Inhibition of transporter-mediated hepatic uptake as a mechanism for drug-drug interaction between cerivastatin and cyclosporin A. *J Pharmacol Exp Ther* **304**: 610-6.

Toshimoto K, Tomaru A, Hosokawa M, Sugiyama Y (2017) Virtual Clinical Studies to Examine the Probability Distribution of the AUC at Target Tissues Using

Physiologically-Based Pharmacokinetic Modeling: Application to Analyses of the Effect of Genetic Polymorphism of Enzymes and Transporters on Irinotecan Induced Side Effects. *Pharm Res* **34**: 1584-1600

Treiber A, Schneiter R, Delahaye S, Clozel M (2004) Inhibition of organic anion transporting polypeptide-mediated hepatic uptake is the major determinant in the pharmacokinetic interaction between bosentan and cyclosporin A in the rat. *J Pharmacol Exp Ther* **308**: 1121-9

Treiber A, Schneiter R, Häusler S, Stieger B (2007) Bosentan is a substrate of human OATP1B1 and OATP1B3: inhibition of hepatic uptake as the common mechanism of its interactions with cyclosporin A, rifampicin, and sildenafil. *Drug Metab Dispos* **35**: 1400-7.

Tsamandouras N, Rostami-Hodjegan A, Aarons L (2015) Combining the 'bottom up' and 'top down' approaches in pharmacokinetic modelling: fitting PBPK models to observed clinical data. *Br J Clin Pharmacol* **79**: 48-55

Ubeaud G, Schmitt C, Jaeck D, Lave T, Coassolo P (1995) Bosentan, a new endothelin receptor antagonist: prediction of the systemic plasma clearance in man from combined in vivo and in vitro data. *Xenobiotica* **25**: 1381-90

Varma MV, Bi Y, Kimito E, Lin J (2014) Quantitative prediction of transporter- and enzyme-mediated clinical drug-drug interactions of organic anion-transporting polypeptide 1B1 substrates using a mechanistic net-effect model. *J Pharmacol Exp Ther* **351**: 214-23

van Giersbergen PL, Halabi A, Dingemanse J (2002) Single- and multiple-dose pharmacokinetics of bosentan and its interaction with ketoconazole. *Br J Clin Pharmacol* **53**: 589-95.

van Giersbergen PL, Treiber A, Schneiter R, Dietrich H, Dingemanse J (2007) Inhibitory and inductive effects of rifampin on the pharmacokinetics of bosentan in healthy subjects. *Clin Pharmacol Ther* **81**: 414-9.

Volz AK, Krause A, Haefeli WE, Dingemanse J, Lehr T (2017) Target-Mediated Drug Disposition Pharmacokinetic-Pharmacodynamic Model of Bosentan and Endothelin-1. *Clin Pharmacokinet* **56**: 1499-1511.

Watanabe T, Kusuhara H, Maeda K, Shitara Y, Sugiyama Y (2009) Physiologically based pharmacokinetic modeling to predict transporter-mediated clearance and distribution of pravastatin in humans. *J Pharmacol Exp Ther* **328**: 652-62.

Watanabe T, Kusuhara H, Sugiyama Y (2010) Application of physiologically based pharmacokinetic modeling and clearance concept to drugs showing transporter-mediated distribution and clearance in humans. *J Pharmacokinet Pharmacodyn* **37**: 575-90

Weber C, Banken L, Birnboeck H, Schulz R (1999) Effect of the endothelin-receptor antagonist bosentan on the pharmacokinetics and pharmacodynamics of warfarin. *J Clin Pharmacol* **39**: 847-54.

Weber C, Gasser R, Hopfgartner G (1999a) Absorption, excretion, and metabolism of the endothelin receptor antagonist bosentan in healthy male subjects. *Drug Metab Dispos* **27**: 810-5.

Weber C, Schmitt R, Birnboeck H, Hopfgartner G, Eggers H, Meyer J, van Marle S,

Viischer HW, Jonkman JH (1999b) Multiple-dose pharmacokinetics, safety, and

tolerability of bosentan, an endothelin receptor antagonist, in healthy male

volunteers. *J Clin Pharmacol* **39**: 703-14.

Weber C, Schmitt R, Birnboeck H, Hopfgartner G, van Marle SP, Peeters PA, Jonkman

JH, Jones CR (1996) Pharmacokinetics and pharmacodynamics of the endothelin-

receptor antagonist bosentan in healthy human subjects. *Clin Pharmacol Ther* **60**:

124-37.

Yoshikado T, Yoshida K, Kotani N, Nakada T, Asaumi R, Toshimoto K, Maeda K,

Kusuhara H, Sugiyama Y (2016) Quantitative analyses of hepatic OATP-mediated

interactions between statins and inhibitors using PBPK modeling with a parameter

optimization method. *Clin Pharmacol Ther* **100**: 513-523.

Yoshikado T, Toshimoto K, Nakada T, Ikejiri K, Kusuhara H, Maeda K, Sugiyama Y

(2017) Comparison of Methods for Estimating Unbound Intracellular-to-Medium

Concentration Ratios in Rat and Human Hepatocytes Using Statins. *Drug Metab

Dispos* **45**: 779-789.

Footnotes

The authors declare no conflicts of interest.

Disclaimer: Although the first author Masanobu Sato is an officer for Pharmaceuticals & Medical Devices Agency (PMDA), the content of this article does not reflect the views or policies of the PMDA or its staff.

Figure legends

Figure 1 The structure of the constructed PBPK model for bosentan after the IV bolus dosing in humans (PS_{act}; transporter-mediated active uptake clearance, $PS_{dif,inf}$; passive diffusion influx clearance from each extrahepatic compartment to hepatocellular compartments, $PS_{dif,eff}$; passive diffusion efflux clearance from each hepatocellular compartment to extrahepatic compartments, $CL_{int,met}$; hepatic intrinsic metabolic clearance, Qt; blood flow rate in tissue, Kp,t; the partition coefficient between these tissues and blood, and CL_r; renal clearance)

Figure 2 Eadie–Hofstee plot of bosentan uptake by cryopreserved human hepatocytes. The initial uptake velocity of bosentan was calculated using the uptake volume obtained between 0.5 and 3 min. The solid line represents the fitted curve via nonlinear least-squares methods. Each point represents the mean ± SD. Internal Figure showed "v vs. c" curve of bosentan uptake by cryopreserved human hepatocytes.

Figure 3 Eadie–Hofstee plots of bosentan metabolism using human microsomes: the production of hydroxyl bosentan (a) and desmethyl bosentan (b). The initial velocity of these metabolites was calculated using the production volume obtained after 3 min incubation. The solid line represents the fitted curve by nonlinear least-squares methods. Each point represents the mean ± SD. Internal Figures showed "v vs. c" curve of bosentan metabolism using human microsomes.

35

Figure 4 Simulation results from the PBPK models (Models 1, 2, 3, 4 and 5) of bosentan.

Solid lines represent the simulation results. The open and closed circles, open and closed

squares, and open triangles indicate the reported bosentan blood concentration-time

profiles with the IV doses of 10, 50, 250, 500, and 750 mg, respectively.

Figure 5 Monte Carlo simulation of bosentan blood concentration profiles

The results of the Monte Carlo simulations that considered interindividual variability in

$V_{max,uptake}$, $K_{m,uptake}$, PS_{dif}, and CL_{met} and intraindividual variability in Model 3. Observed

mean and standard of error values of each dose are shown as closed circles and lines and

mean values of dose-normalized AUCs of each virtual study estimated from Monte Carlo

simulation using Model 3 are indicated as closed rectangles.

Table 1 Physiological and kinetic parameters used for PBPK modeling (the kinetic parameters experimentally obtained from *in vitro* studies presented as the mean ± SD).

Parameters	Value	Source
Physiological parameters		
Body Weight (kg)	78	Weber et al., 1996
Hepatocellular space (g/kg)	6.69	Davies and
Extrachepatic space (g/kg)	17.4	Morris, 1993
Adipose (g/kg)	142	
Muscle (g/kg)	429	
Skin (g/kg)	111	
Blood flow rate		
Liver (mL/min/kg)	20.7	Davies and Morris, 1993
Adipose (mL/min/kg)	3.72	
Muscle (mL/min/kg)	10.7	
Skin (mL/min/kg)	4.28	
Tissue/blood concentration ratio		
Adipose	0.121	Calculated from Reported
Muscle	0.119	Equations
Skin	0.483	(Rodgers and Rowland, 2006)
Kinetic parameters		
Plasma unbound fraction	0.02	Dingemanse and van
Blood/plasma concentration ratio	0.6	Giersbergen, 2004
Renal clearance (L/hr)	0.144	Weber et al., 1996
$V_{\text{max, uptake}}$ (pmol/min/10^6 cells)	47.4 ± 18.6	Current study
$K_{\text{m, uptake}}$ (μM)	1.33 ± 1.34	
$PS_{\text{dif,inf}}$ (pmol/min/10^6 cells)	2.89 ± 0.46	
$V_{\text{max, met,OH}}$ (pmol/min/mg microsomal protein)	16.4 ± 1.75	
$K_{\text{m, met,OH}}$ (μM)	6.40 ± 1.20	

$CL_{met,OH,nonsaturable}$ (µL/min/ mg microsomal protein)	0.158 ± 0.015
$V_{max, met,DES}$ (pmol/min/mg microsomal protein)	7.53 ± 2.39
$K_{m, met,DES}$ (µM)	4.80 ± 2.61
$CL_{met,DES,nonsaturable}$ (µL/min/ mg microsomal protein)	0.273 ± 0.025
f_H	0.0696 ± 0.0068

$V_{max, uptake}$, V_{max} for the transporter-mediated hepatic uptake; $K_{m, uptake}$, K_m value for the transporter-mediated hepatic uptake; $PS_{dif,inf}$, passive diffusion influx clearance; V_{max, met_OH}, V_{max} for the production of hydroxyl bosentan; K_{m, met_OH}, K_m value for the production of hydroxyl bosentan; nonsaturable $CL_{,met\_OH}$, nonsaturable metabolic clearance for the production of hydroxyl bosentan; V_{max, met_DES}, V_{max} for the production of desmethyl bosentan; K_{m, met_DES}, K_m value for the production of desmethyl bosentan; nonsaturable $CL_{,met\_DES}$, nonsaturable metabolic clearance for the production of desmethyl bosentan; f_H, hepatic intracellular unbound fraction

Table 2 Comparison of the PBPK models used in the current study

	Bottom-up approach		Top-down approach		
	Model	Model	Model	Model	Models
	1	2	3	4	5
Scaling factors for hepatic transport and metabolism	Biological scaling factors	Obtained by fitting			
Incorporation of saturable hepatic uptake			Yes		Yes
Incorporation of saturable hepatic metabolism				Yes	Yes
Fitted parameters			*in vivo* parameters of $V_{\text{max,uptake}}$, $K_{\text{m,uptake}}$, $PS_{\text{dif,inf}}$, $CL_{\text{int,met}}$, and V_{c}	*in vivo* parameters of PS_{act}, $PS_{\text{dif,inf}}$, $V_{\text{max,met}}$, $K_{\text{m,met}}$ and V_{c}	*in vivo* parameters of $V_{\text{max,uptake}}$, $K_{\text{m,uptake}}$, $PS_{\text{dif,inf}}$, $V_{\text{max,met}}$, $K_{\text{m,met}}$ and V_{c}

Table 3 Parameter values used for PBPK modeling.

Each parameter presented as the mean ± SD. * Range is the constraint on the estimates for each parameter in model fitting to data.

Parameters	Units	Model					Initial value
		1	2	3	4	5	(Range*)
$V_{max, uptake}$	μmol/hr/78 kg	642	642	1610 ± 159		1750 ± 364	642 (64.2-6420)
$K_{m, uptake}$	μM	1.33	1.33	0.534 ± 0.0845		0.667 ± 0.132	1.33 (> 0.001)
PS_{act}	L/hr/78 kg				2360 ± 629		483 (48.3-4830)
$PS_{dif,inf}$	L/hr/78 kg	39.1	39.1	5.05 ± 0.729	5.35 ± 2.11	4.22 ± 1.04	39.1 (3.91-391)
$PS_{dif,eff}$ [a]	L/hr/78 kg	161	161	20.8	22.0	17.4	
$V_{max, met,OH}$	μmol/hr/78 kg	97.1	97.1				
$K_{m, met,OH}$	μM	6.4	6.4				
$CL_{met,OH,nonsaturable}$	L/hr/78 kg	0.936	0.936				
$V_{max, met,DES}$	μmol/hr/78 kg	44.6	44.6				
$K_{m, met,DES}$	μM	4.8	4.8				
$CL_{met,OH,nonsaturable}$	L/hr/78 kg	1.62	1.62				
$V_{max, met}$	μmol/hr/78 kg				868 ± 438	1140 ± 713	135 (13.5-1350)
$K_{m, met}$	μM				108 ± 59.4	163 ± 106	5 (>0.001)

40

$CL_{int,met}$	L/hr/78 kg			6.77 $\pm$ 0.404			27 (2.7-270)
$SF,transport$			10.0 $\pm$ 47				1 (0.1-10)
SF,met			10.0 $\pm$ 6.5				1 (0.1-10)
V_c	L/78 kg	6.3	10.5 $\pm$ 2.89	7.43 $\pm$ 0.953	6.93 $\pm$ 2.54	6.94 $\pm$ 1.06	6.3 (5.25-10.5)
final WSS			28.5816	3.01871	6.84816	3.48	
AIC			207.166	76.290	125.439	86.8143	

a Caluculated by $PS_{dif,inf}$ and γ

$V_{max, uptake}$, V_{max} for the transporter-mediated hepatic uptake; $K_{m, uptake}$, K_m value for the transporter-mediated hepatic uptake; PS_{act}, intrinsic clearance of transporter-mediated hepatic uptake; PS_{dif}, passive diffusion clearance; V_{max, met_OH}, V_{max} for the production of hydroxyl bosentan; K_{m, met_OH}, K_m value for the production of hydroxyl bosentan; nonsaturable $CL_{,met\_OH}$, nonsaturable metabolic clearance for the production of hydroxyl bosentan; V_{max, met_DES}, V_{max} for the production of desmethyl bosentan; K_{m, met_DES}, K_m value for the production of desmethyl bosentan; nonsaturable $CL_{,met\_OH}$, nonsaturable metabolic clearance for the production of desmethyl bosentan; $V_{max, met}$, V_{max} for bosentan metabolism; $K_{m, met}$, K_m value for bosentan metabolism; $CL_{int,met}$, metabolic clearance of bosentan; "SF, transport", scaling factors for $V_{max,uptake}$ and PS_{dif}; "SF, met", scaling factors for $V_{max,met\_OH}, V_{max,met\_DES}$, CL_{met}; and V_c, distribution volume of the central compartment

41

Fig. 1

Adipose

Muscle

Skin

Q_a
$K_{p,a}$

Q_m
$K_{p,m}$

Q_s
$K_{p,s}$

CL_r

Central

Q_h

Extrahepatic

EH 1 → EH 2 → EH 3 → EH 4 → EH 5

$PS_{act} + PS_{dif,inf}$

$PS_{dif,eff}$

Hepatocellular

HC 1   HC 2   HC 3   HC 4   HC 5

$CL_{int,met}$

Fig. 2

Fig. 3

A)

B)
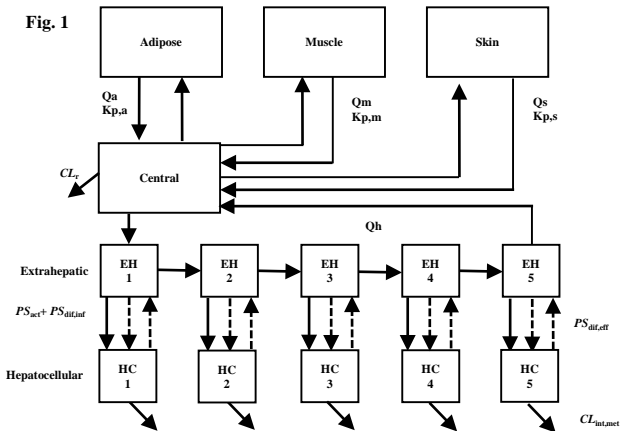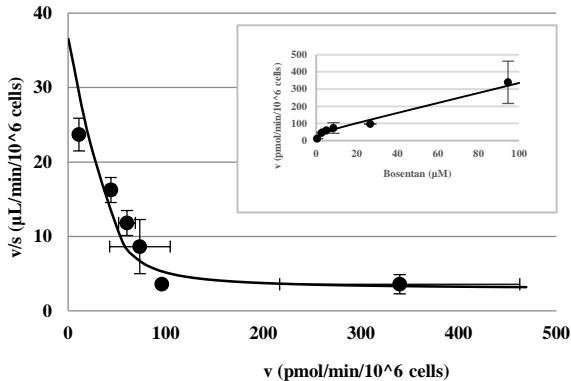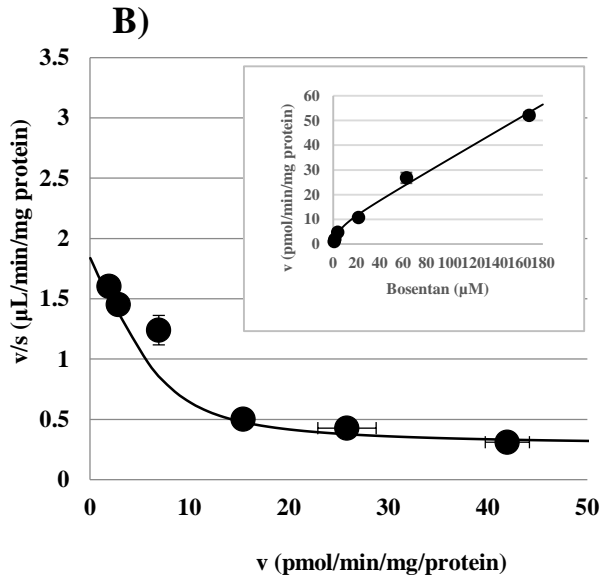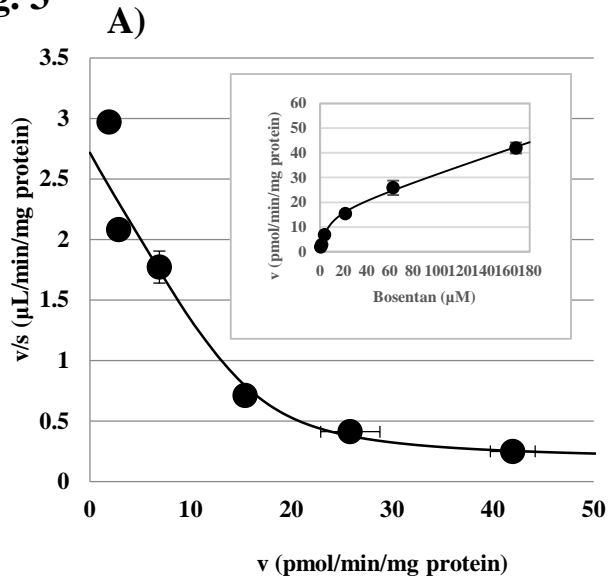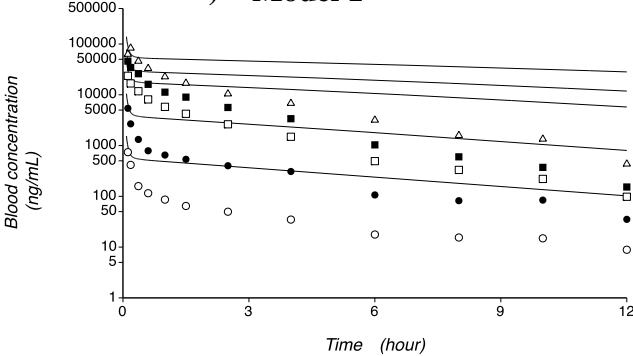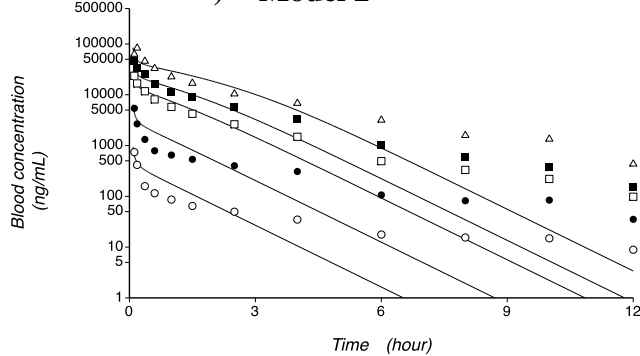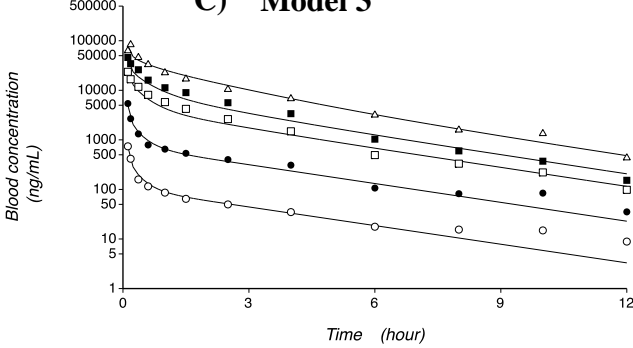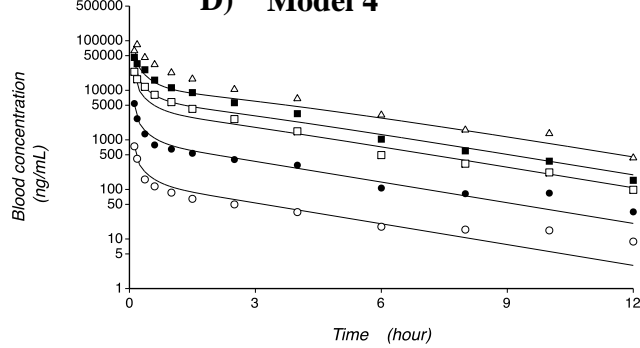
Fig. 4

A) Model 1

B) Model 2

C) Model 3

D) Model 4

E) Model 5
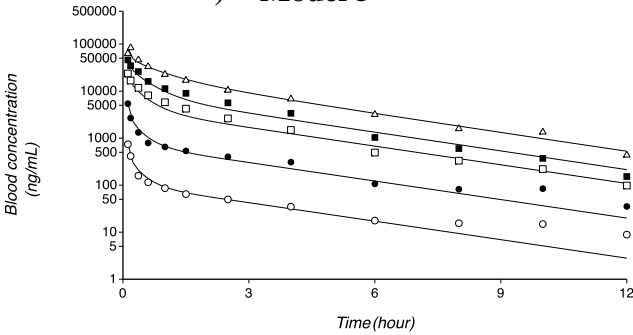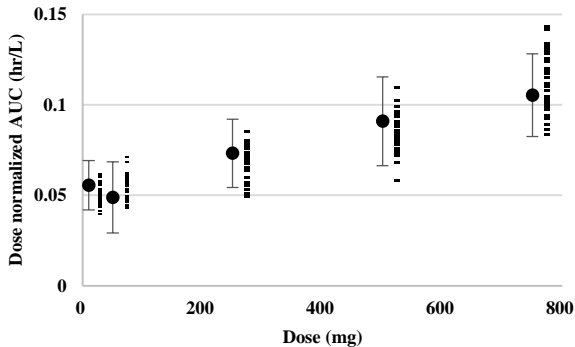
Fig. 5

Supplementary File

Article's Title;

Physiologically Based Pharmacokinetic Modeling of Bosentan Identifies the Saturable

Hepatic Uptake as A Major Contributor to Its Nonlinear Pharmacokinetics

Authors;

Masanobu Sato, Kota Toshimoto, Atsuko Tomaru, Takashi Yoshikado, Yuta Tanaka,

Akihiro Hisaka, Wooin Lee and Yuichi Sugiyama

Journal Title;

Drug Metabolism and Disposition

Supplementary text 1

In our constructed PBPK model, the concentration profile of bosentan in each

compartment can be expressed by the following differential equations.

Central:

$$V_c \frac{dC_c}{dt} = Q_h(C_{EH5} - C_c) + Q_a\left(\frac{C_a}{K_{p,a}} - C_c\right) + Q_m\left(\frac{C_m}{K_{p,m}} - C_c\right) + Q_s\left(\frac{C_s}{K_{p,s}} - C_c\right)$$
$$- CL_r \, C_c$$

(V, volume; C, concentration; Q, blood flow rate of each organ; subscript c, h, a, m, and

s, the compartment of central, hepatic, adipose, muscle and skin, respectively; EH5, the

fifth extrahepatic compartment)

Hepatocyte compartments 1 to 5:

$$\frac{1}{5}V_{HCi}\left(\frac{dC_{HCi}}{dt}\right) = \frac{1}{5}\{(PS_{act} + PS_{dif,inf})f_B C_{HEi} - (PS_{dif,eff} + CL_{int,met})f_H C_{HCi}\}$$

Hepatic extracellular compartment 1:

$$\frac{1}{5}V_{HE1}\left(\frac{dC_{HE1}}{dt}\right) = Q_h(C_c - C_{HE1}) + \frac{1}{5}\{PS_{dif,eff}f_H C_{HC1} - (PS_{act} + PS_{dif,inf})f_B C_{HE1}\}$$

(HC1, the first hepatocellular compartment; f_B, the unbound fraction in blood)

Hepatic extracellular compartments 2 to 5:

2

$$\frac{1}{5}V_{HEi}\left(\frac{dC_{HEi}}{dt}\right)$$

$$= Q_h\big(C_{HE(i-1)} - C_{HEi}\big)$$

$$+ \frac{1}{5}\{PS_{dif,eff}\, f_H C_{HCi} - (PS_{act} + PS_{dif,inf})f_B C_{HEi}\}$$

(subscript i,   the number of the compartment)

Non-elimination organ (adipose, muscle and skin):

$$V_a \frac{dC_a}{dt} = Q_a(C_c - \frac{1}{K_{p,a}}C_a)$$

$$V_m \frac{dC_m}{dt} = Q_m \left(C_c - \frac{1}{K_{p,m}} C_m \right)$$

$$V_s \frac{dC_s}{dt} = Q_s(C_c - \frac{1}{K_{p,s}}C_s)$$

For bottom-up approaches (Models 1 and 2), the metabolism of bosentan into both

hydroxyl bosentan and desmethyl bosentan was taken into consideration. PS_{act}, $PS_{dif,inf}$

and $CL_{int,met}$ were expressed by the following equations.

$$PS_{act} = \frac{In\ vitro\ V_{max,uptake} \times SF_{uptake}}{In\ vitro\ K_{m,uptake} + f_B C_{HEi}}$$

$$PS_{dif,inf} = In\ vitro\ PS_{dif,inf} \times SF_{uptake}$$

$$CL_{int,met} = \Bigg(\frac{In\ vitro\ V_{max,met,OH}}{In\ vitro\ K_{m,met,OH} + f_H C_{HCi}} + In\ vitro\ CL_{met,OH,nonsaturable}$$

$$+ \frac{In\ vitro\ V_{max,met,DES}}{In\ vitro\ K_{m,met,DES} + f_H C_{HCi}} + In\ vitro\ CL_{met,DES,nonsaturable}\Bigg)$$

$$\times SF_{met}$$

where SF_{uptake} and SF_{met} were calculated based on 1.2×10^8 hepatocytes/g of liver, 24.1 g of liver/kg body, and 52.5 mg microsomal protein/g of liver (Davies and Morris, 1993; Iwatsubo et al., 1997). In the simulation analysis, the central compartment volume (V_c) was assumed to be 6.3 L/78 kg. In Model 2, the SF_{uptake}, SF_{met}, and V_c were optimized to fit the bosentan blood concentration profiles of the intravenous bosentan doses from 10 to 750 mg. In these analyses (Models 1 and 2), the values of $V_{max,uptake}$, $K_{m,uptake}$, $PS_{dif,inf}$, kinetic parameters representing the production of hydroxyl bosentan including $V_{max,met,OH}$, $K_{m,met,OH}$ and $CL_{met,OH,nonsaturable}$, and kinetic parameters representing the production of desmethyl bosentan including $V_{max,met,DES}$, $K_{m,met,DES}$, and $CL_{met,DES,nonsaturable}$ were fixed to the values from the *in vitro* kinetic parameters.

For top-down approaches (Models 3, 4 and 5), we performed simultaneous fitting analyses of the PBPK models that incorporate saturable processes for PS_{act}, $CL_{int,met}$ or both to bosentan blood concentration profiles. In Models 3, 4 and 5, the following parameters were optimized;

    (1) Model 3

In vivo $V_{max,uptake}$, *in vivo* $K_{m,uptake}$, *in vivo* $PS_{dif,inf}$, *in vivo* $CL_{int,met}$, and V_c

    (2) Model 4

in vivo PS_{act}, *in vivo* $PS_{dif,inf}$, *in vivo* $V_{max,met}$, *in vivo* $K_{m,met}$ and V_c

    (3) Model 5

In vivo $V_{max,uptake}$, *in vivo* $K_{m,uptake}$, *in vivo* $PS_{dif,inf}$, *in vivo* $V_{max,met}$, *in vivo* $K_{m,met}$ and V_c

The initial values of these fitting parameters were determined using the following methods: *in vivo* $V_{\text{max,uptake}}$ and *in vivo* PS_{dif} were extrapolated biologically from *in vitro* parameters described above; *in vivo* $K_{\text{m,uptake}}$ was set at the equivalent with *in vitro* $K_{\text{m,uptake}}$ values; *in vivo* PS_{act} was determined by calculating *in vivo* $V_{\text{max,uptake}}$/*in vivo* $K_{\text{m,uptake}}$ assuming a linear condition in which $f_B C_{\text{HEi}}$ was much lower than *in vivo* $K_{\text{m,uptake}}$; *in vivo* $CL_{\text{int,met}}$ was calculated by the sum of *in vivo* $V_{\text{max,met,OH}}/K_{\text{m,met,OH}}$, $CL_{\text{met,OH,nonsaturable}}$, $V_{\text{max,met,DES}}/K_{\text{m,met,DES}}$, and $CL_{\text{met,DES,nonsaturable}}$; *in vivo* $K_{\text{m,met}}$ was set at 5 μM according to *in vitro* $K_{\text{m,met,OH}}$ and $K_{\text{m,met,DES}}$; *in vivo* $V_{\text{max,met}}$ was determined by the calculation of *in vivo* CL_{met} and *in vivo* $K_{\text{m,met}}$; and V_c were set at 6.3 L/78 kg, respectively.

Supplementary text 2

Efforts to apply the PBPK model to reproduce pharmacokinetic profiles following oral bosentan dosing

The reported pharmacokinetic profiles of orally administered bosentan display deviations from dose-proportional behaviors, but in the opposite direction to the results of intravenously administered bosentan (Supplementary Figure 2). The dose-normalized AUCs of orally administered (as 100 ml aqueous suspension) showed a decreasing trend as the bosentan doses increased from 3 to 2,400 mg (Clin Pharmacol Ther 60: 124-37). This decreasing trend with oral bosentan dosing may arise from multiple mechanisms including the saturation in plasma protein binding, solubility, and/or uptake transporters (e.g. OATP2B1) expressed in the luminal side of enterocytes. To obtain mechanistic insights, we attempted to establish a PBPK model that can capture non-linear pharmacokinetic behavior of orally administered bosentan.

To develop a PBPK model for orally administered bosentan, several modifications were incorporated. First, the ADAM (Advanced Dissolution, Absorption and Metabolism) model was incorporated into the systemic PBPK model using SimCYP (version 16.0, SimCYP Ltd, Sheffield, UK, Supplementary Figure 3). The kinetic parameters are described in Supplementary Table 1 (V_{max} for CYP2C9 or CYP3A4, J_{max} for OATP1B1, and K_p scalar were re-optimized to reproduce the bosentan concentration-time profiles following intravenous bolus dosing). The following saturable components were also

6

incorporated into the PBPK model: i) hepatic efflux ($PS_{dif,eff}$) ii) intestinal solubility-pH

profiles (reported in the interview form, Supplementary Figure 4), iii) intestinal efflux

(by P-glycoprotein, obtained from Caco-2 permeability experiments with and without

100 μM verapamil), iv) intestinal uptake (by OATP2B1, obtained from the uptake study

using HEK293 cells expressing OATP2B1). The possibility of supersaturation of

bosentan in oral dosing solution (100 mL aqueous suspension) was also considered (the

solubility of bosentan was described to be 0.01 mg/mL in the interview). Given each

oral bosentan dose was given as 100 mL aqueous suspension, the fraction of API

dissolved for each dose was set as described in Supplementary Table 2. Two cases of

simulations were performed with the critical supersaturation ratio of 1 and 10,

respectively, using SimCYP. For each case, the simulation was performed with J_{max} of

OATP2B1 = 0, 5, 15, and 45 pmol/min, respectively in 100 virtual subjects generated

from Sim-Healthy Volunteers.

The constructed PBPK model reasonably reproduced the non-linear pharmacokinetic

profiles of intravenously administered bosentan (Supplementary Figure 5). However, it

was not the case for orally administered bosentan, regardless of the consideration of the

supersaturation of bosentan (Supplementary Figures 6 and 7). With low bosentan doses

(3 – 100 mg), the simulation results were in a relatively good agreement with the

reported profiles when J_{max} of OATP2B1 was set as 0 (i.e. no consideration of

OATP2B1 uptake). However, the simulation results showed substantial deviations from

the reported profiles for high bosentan doses (600 - 2,400 mg), regardless of the

consideration of apical uptake for OATP2B1.

Legends for Supplementary Figures

Supplementary Figure 1 Simulated Bosentan Concentration in Hepatocyte
Compartment 1 by Model 3, 4 and 5

Supplementary Figure 2 Relationship between bosentan doses and the dose-
normalized AUCplasma following intravenous (A) or oral (B) dosing
Error bars show the standard deviation.

Supplementary Figure 3 Structure of a PBPK model for orally administered bosentan
The ADAM (Advanced dissolution, absorption and metabolism) model was used for
intestinal absorption of bosentan using SimCYP version 16.0.

Supplementary Figure 4 Solubility-pH profiles of bosentan
Square symbols represent the observed data in the interview form. Three colored curves
represent simulated solubility-pH profiles; red, using in silico estimated pKa (= 4.0) and
the intrinsic solubility (Sunionized, 0.0038mg/mL); green, using pKa (= 5.1) and
Sunionized, (= 0.001mg/mL) described in the interview form; blue, using optimized
pKa (= 5.4) and Sunionized, (= 0.0011mg/mL).

Supplementary Figure 5 (A) Mean plasma bosentan concentration-time profiles
following intravenous dosing of various bosentan doses: 10 mg (black), 68 mg (purple),
308 mg (green), 500 mg (blue), and 904 mg (red), respectively. Solid symbols represent
the observed mean values while the solid lines represent simulation results in 100
virtual subjects.
(B) Comparison of dose-normalized AUCs between the observed and predicted values
Red and blue symbols represent the simulated and observed values, respectively. Error
bars show the standard deviation.

Supplementary Figure 6 Plasma concentration-time profiles of orally administered
bosentan without consideration of supersaturation (critical supersaturation ratio = 1)
The Jmax values of OATP2B1 are set as 0 (A), 5 (B), 15 (C) and 45 (D) pmol/min,
respectively. Solid symbols represent the observed mean values while the lines represent
simulation results. Black, 3 mg; purple, 10 mg; blue, 30mg; red, 100 mg; black, 300 mg;
purple, 600 mg; blue, 1,200 mg; red, 2,400 mg.

Supplementary Figure 7 Plasma concentration-time profiles of orally administered bosentan considering supersaturation (critical supersaturation ratio = 10)
The Jmax values of OATP2B1 are set as 0 (A), 5 (B), 15 (C) and 45 (D) pmol/min, respectively. Solid symbols represent the observed mean values while the lines represent simulation results. Black, 3 mg; purple, 10 mg; blue, 30mg; red, 100 mg; black, 300 mg; purple, 600 mg; blue, 1,200 mg; red, 2,400 mg.

Supplementary table 1

Input parameters for bosentan in SimCYP

Category	Parameters	Units	Value	Comments
Phys Chem and Blood Binding	molecular weight	g/mol	551.61	
	Log Po:w		3.4	
	pKa		Monoprotic Acid 5.4	Estimated from solubility-pH profile
	B/P		0.6	
	fraction unbound in plasma		0.02	
Absorption	Absorption model		ADAM model	
	$P_{eff,man}$	10-4cm/s	2.34	Calculated from in house Caco-2 permeability experiment data
	Formulation type		Suspension	
	Fraction API Dissolved	%	See Supplementary Table 1b	

	Aqueous Phase Solubility	mg/mL	Solubility-pH Profile	Solubility-pH profile is shown in Supplementary Table 1c
	Kinetic Solubility		Model 2	
	Critical Supersaturation Ratio		1, 10	1; no consideration of supersaturation 10; default value in SimCYP
Distribution	Distribution model		Full PBPK	
	Vss prediction method		Method 3	
	V_{ss}	L/kg	0.26	
	K_p scalar		3.54	Estimated using bonsentan i.v. concentration time profile
Elimination	Elimination model	Enzyme kinetics		
	HLM CYP2C9 K_m	μM	6.4	Set $K_{m,met,OH}$ value in Table 1
	HLM CYP2C9 V_{max}	pmol/min/mg protein	59.9	Estimated using bonsentan i.v. concentration time profile

	HLM CYP3A4 K_m	µM	4.8	Set $K_{m,met,DES}$ value in Table 1
	HLM CYP3A4 V_{max}	pmol/min/mg protein	67.4	Estimated using bonsentan i.v. concentration time profile
	CL_R	L/h	0.0864	Renal clearance described in Table 1 (0.144 L/h) * B/P (0.6) = 0.0864
Transport	(Liver)			
	CL_{PD}	mL/min/million hepatocytes	0.00289	Set $PS_{dif,inf}$ value in Table 1
	fu_{IW}		0.0696	Set f_H value in Table 1
	OATP1B1 Km	µM	1.33	Set $K_{m,uptake}$ value in Table 1
	OATP1B1 J_{max}	pmol/min/million cells	179	estimated using bonsentan i.v. concentration time profile
	Sinusoidal Efflux $CL_{int,T}$	µL/min/million cells	7.65	The difference between $PS_{dif,eff}$ and $PS_{dif,inf}$ ($PS_{dif,inf}$ * (γ - 1))
	(Intestine)			
	P-gp K_m	µM	4.09	in-house study
	P-gp J_{max}	pmol/min	124	in-house study

P-gp A	cm^2	1	in-house study
P-gp System		Caco-2	in-house study
			in-house study
Apical uptake K$_m$	μM	0.421	OATP2B1 was considered as an apical uptake transporter.
Apical uptake J$_{max}$	pmol/min	0, 5, 15, 45	
Apical uptake A	cm^2	1	
Apical uptake System		User	

Supplementary Table 2

Fraction of API dissolved value for each dose of bosentan

Bosentan dose (mg)	Fraction of API dissolved (%)
3	33
10	10
30	3.3
100	1.0
300	0.33
600	0.17
1200	0.083
2400	0.042

Supplementary Table 3

Solubility-pH profile of bosentan described in the interview form

pH	Solubility (mg/mL)
4	0.001
5	0.002
7.5	0.43
8	0.53
8.5	0.93

Supplementary Fig. 1
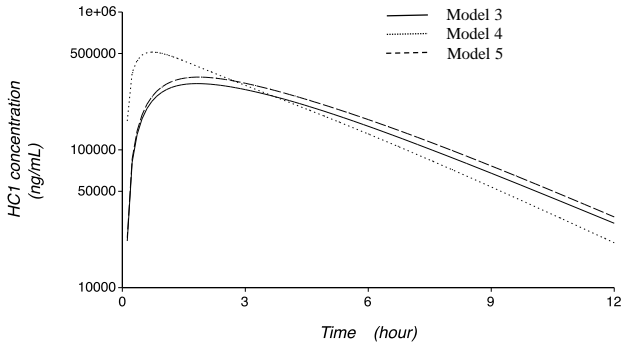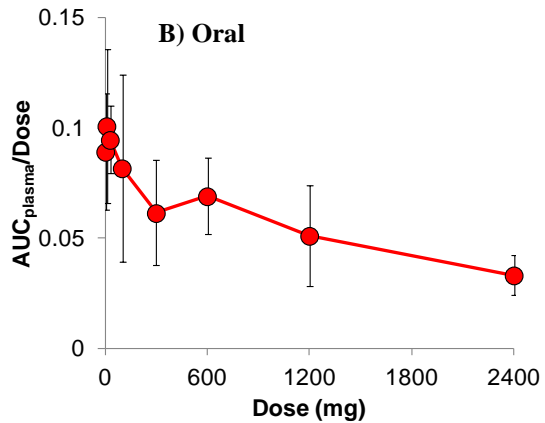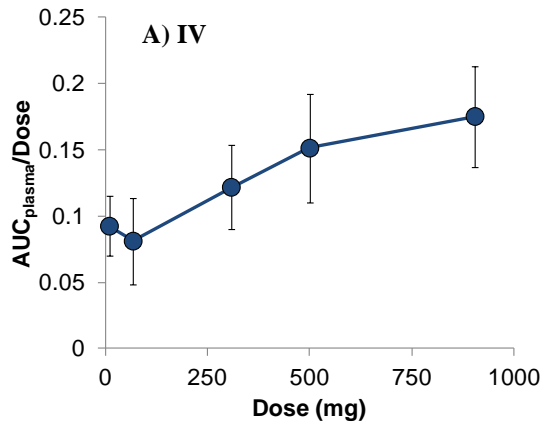
Supplementary Fig. 3
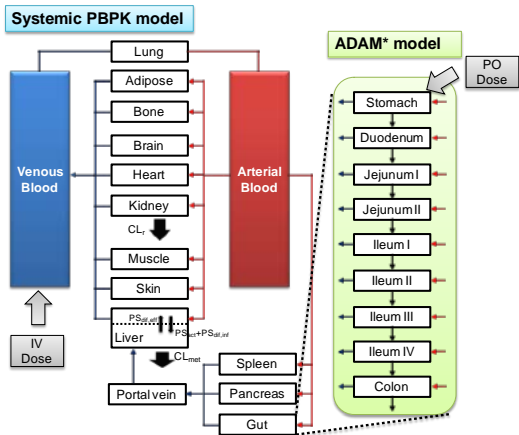
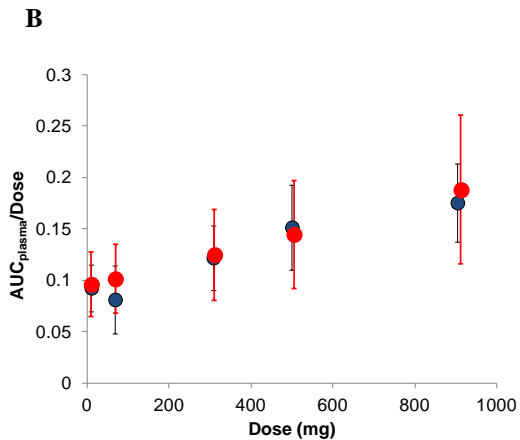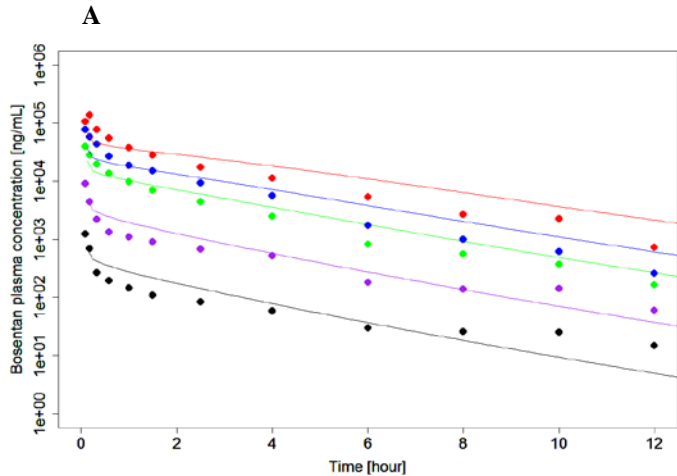**Supplementary Fig. 4**
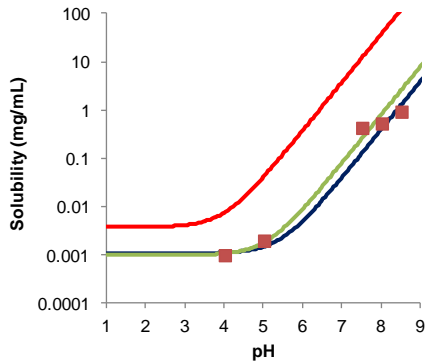
Supplementary Fig. 5

A

B
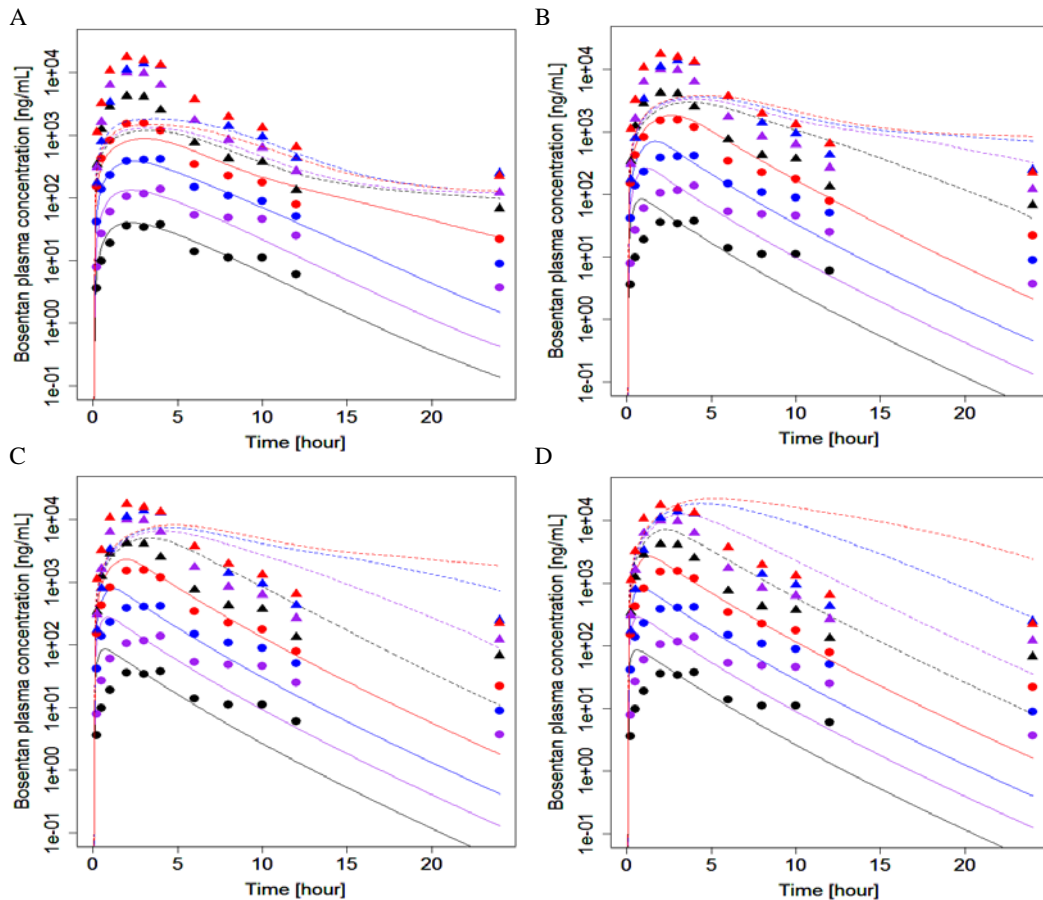
Supplementary Fig. 6

Supplementary Fig. 7